J Physiol (2003), **548.3**, *pp.* 753–764
DOI: 10.1113/jphysiol.2002.037036

www.jphysiol.org

Journal of Physiology

Intraterminal Ca^{2+} concentration and asynchronous transmitter release at single GABAergic boutons in rat collicular cultures

Sergei Kirischuk and Rosemarie Grantyn

Developmental Physiology, Johannes Müller Institute of Physiology, Humboldt University Medical School (Charité), 10117 Berlin, Germany

Neurotransmitter release in response to a single action potential has a precise time course. A significant fraction of the releasable vesicles is exocytosed synchronously, within a few milliseconds after the arrival of an action potential. If repeatedly activated, stimulus-locked phasic synchronous release declines, but synaptic transmission can be maintained through tonic asynchronous transmitter release. The desynchronisation of release during repetitive activation is generally attributed to a build-up of intraterminal Ca^{2+} concentration. However, the precise relationship between presynaptic Ca^{2+} level and asynchronous release rate at small central synapses has remained unclear. Here we characterise this relationship for single GABAergic terminals in rat collicular cultures. In the presence of tetrodotoxin, inhibitory postsynaptic currents (IPSCs) and presynaptic Ca^{2+} transients were recorded in response to direct presynaptic depolarisation of individual boutons. Repetitive stimulation indeed resulted in a shift from phasic to asynchronous neurotransmitter release. A clear dominance of the asynchronous release mode was observed after 10 pulses. The steady-state asynchronous release rate showed a third-power dependency on the presynaptic Ca^{2+} concentration, which is similar to that of evoked release. The Ca^{2+} sensor for asynchronous release exhibited a high affinity for Ca^{2+} and was far from saturation. These properties of the Ca^{2+} sensor should make the asynchronous release very sensitive to any modification of presynaptic Ca^{2+} concentration, including those resulting from changes in presynaptic activity patterns. Thus, asynchronous release represents a powerful but delicately regulated mechanism that ensures the maintenance of appropriate inhibition when the readily releasable pool of vesicles is depleted.

(Resubmitted 4 December 2002; accepted after revision 18 February 2003; first published online 14 March 2003)
Corresponding author S. Kirischuk: Universitätsklinikum Charite, Johannes Müller Institut für Physiologie, Tucholsky Str. 2, 10117 Berlin, Germany. Email: sergei.kirischuk@charite.de

The invasion of a synaptic terminal by an action potential results in a rapid increase of presynaptic Ca^{2+} concentration ($[Ca^{2+}]_{pre}$). The latter triggers the fusion of synaptic vesicles with the synaptic plasma membrane and the release of neurotransmitter into the synaptic cleft (Katz, 1969). This phasic release is thought to be triggered by a brief, localised $[Ca^{2+}]$ increase in the vicinity of open, presynaptic Ca^{2+} channels. Unfortunately, the rapidly decaying, local Ca^{2+} signal that triggers vesicle fusion in presynaptic terminals cannot be resolved with the imaging techniques available. Modelling studies predicted that the Ca^{2+} sensor for vesicle fusion is activated by local $[Ca^{2+}]_{pre}$ elevations above 100 μM (Simon & Llinas, 1985; Zucker & Fogelson, 1986; Augustine *et al.* 1991; Llinas *et al.* 1995; Neher, 1998). However, the Ca^{2+} dependence of transmitter release is determined not only by the Ca^{2+} affinities of the Ca^{2+} sensors, but also by the topography of the sites of Ca^{2+} influx and Ca^{2+} sensors (Meinrenken *et al.* 2002). Recently, the Ca^{2+} sensitivity of glutamate release was measured directly in a giant synapse in the auditory brainstem (the calyx of Held) using laser (Bollmann *et al.* 2000) or flash (Schneggenburger & Neher, 2000) Ca^{2+} photolysis. The results showed that a step-like $[Ca^{2+}]_{pre}$ elevation to only 10 μM was sufficient to induce fast transmitter release with the capacity to deplete about 80 % of the available vesicle pool.

In contrast to large synapses, like the calyx of Held, most axonal terminals in the central nervous system (CNS) are small, with a typical volume of about 1 μm^3. This miniaturisation imposes constraints on studies of transmitter release. Therefore, a quantitative description of the Ca^{2+} dependence of phasic release in small CNS terminals remains problematic. However, in many preparations, rapid phasic release is followed by a tail of miniature-like events (del Castillo & Katz, 1954; Goda & Stevens, 1994; Ravin *et al.* 1997; Atluri & Regehr, 1998; Jensen *et al.* 2000; Lu & Trussell, 2000; Oleskevich & Walmsley, 2002). This delayed release is driven by bulk $[Ca^{2+}]_{pre}$ (Kamiya & Zucker, 1994; Cummings *et al.* 1996; Ravin *et al.* 1997; Jensen *et al.* 2000). Furthermore, during repetitive firing or stimulation (i.e. under conditions that

lead to depletion of the readily releasable vesicle pool, RRP), synapses may switch to the asynchronous mode of release (Lu & Trussell, 2000). When the stimulation is long enough, both $[Ca^{2+}]_{pre}$ and the rate of vesicle release reach a steady-state level. This offers an opportunity to investigate the relationship between $[Ca^{2+}]_{pre}$ and asynchronous release under quasi-stationary conditions. Using this approach, the affinity of the Ca^{2+} sensor for asynchronous release in neuromuscular junctions was shown to be in a lower micromolar range (Ravin *et al.* 1997; Angleson & Betz, 2001).

In low-density cultures from central nervous structures, individual boutons can be selectively activated by focal electrical stimulation. Simultaneous recordings of presynaptic Ca^{2+} responses and respective inhibitory GABAergic postsynaptic currents (IPSCs) provide an opportunity to shed light on the link between pre- and postsynaptic sites at individual inhibitory synaptic contacts (Kirischuk *et al.* 1999*a*,*b*, 2002; Kirischuk & Grantyn, 2002). The present work pursued two goals: (1) to determine the activation patterns that lead to a shift from phasic to asynchronous neurotransmitter release, and (2) to estimate the Ca^{2+} sensitivity of asynchronous release.

METHODS

Cultures

Cell cultures were prepared as described before (Perouansky & Grantyn, 1989). Neonatal rats were anaesthetised with ether before decapitation. The superior colliculi of embryonic day 21 rats were removed and dissociated. The neurones were grown at low density (about 5000 cells cm^{-2}) on laminin-coated glass coverslips. Experiments were performed on cultures between 14 and 21 days *in vitro*. All experiments were carried out according to the guidelines laid down by the Landesamt für Arbeitsschutz, Gesundheitsshutz und technische Sicherheit Berlin (T0406/98).

Imaging

A detailed description of the method used is given elsewhere (Kirischuk *et al.* 1999*b*). Briefly, cultures were incubated in standard extracellular solution (mM: 140 NaCl, 3 KCl, 1 $MgCl_2$, 2 $CaCl_2$, 20 Hepes, 30 glucose; pH set to 7.4 with NaOH) supplemented with either Magnesium Green-AM (MG-AM) or Oregon Green 488 BAPTA-5N-AM (OGB-5N-AM, 5 μM, 30 min at 36 °C) and then kept for an additional 20 min in standard saline to ensure de-esterification. Next, synaptic vesicles were stained with a fluorescent marker. FM4-64 was loaded in two steps. Cultures were incubated first in solution containing high K^+ (50 mM) and FM4-64 (10 μM) for 1 min, and were then switched to extracellular solution containing FM4-64 (10 μM) for a further 1 min, before being washed twice in extracellular solution alone. The coverslip with the stained cultures formed the bottom of a recording chamber on the stage of an inverted microscope (Axiovert 100, Zeiss, Jena, Germany). A × 100 phase contrast, oil-immersion objective with a numerical aperture of 1.3 (Zeiss) was used in all experiments. The excitation wavelengths were controlled by a fast monochromator system, and fluorescence signals were recorded using a CCD camera (TILL Photonics, Munich, Germany). All measurements were performed using 4 × 4 binning (1 pixel = 0.4 μm × 0.4 μm). The acquisition rate for $[Ca^{2+}]$ measurement was one image per 50 ms. The probes were excited at 490 nm. The excitation and emission light was separated using a 510 nm dichroic mirror. The emitted light was filtered at 550 ± 30 nm for Ca^{2+}-sensitive probes and at 600 nm for FM4-64. Phase contrast and FM4-64 images were captured at the beginning of each experiment. The FM4-64 image was converted to binary format using a threshold set to half-maximal intensity above the background. The binary image was used as a mask (by multiplication) to define the presynaptic region of interest for subsequent MG or OGB-5N images. The background fluorescence originating from glial cells was calculated from a region in the immediate vicinity of the stimulated bouton and subtracted. To decrease contamination of the presynaptic signal by fluorescence from the underlying dendrite, all measurements were performed after at least 15 min dialysis of the postsynaptic neurone. Fluorescence signals are expressed as the relative change from the prestimulus level ($\Delta F/F_0$).

Patch-clamp recordings

Whole-cell patch-clamp recordings were performed using glass pipettes containing (mM): 100 potassium gluconate, 50 KCl, 5 NaCl, 2 $MgCl_2$, 1 $CaCl_2$, 10 EGTA and 20 Hepes; the pH was set to 7.2 with KOH. The holding potential was −70 mV, and the E_{Cl} was about −20 mV. Signals were acquired at 10 kHz using an EPC-7 patch-clamp amplifier and TIDA 3.7 acquisition software (HEKA Electronics, Lambrecht/Pfalz, Germany). Series resistance (10–25 MΩ) was compensated up to 70 %.

Selection and stimulation of synaptic boutons

All experiments were carried out on well-isolated GABAergic axodendritic boutons (about 1 μm in diameter) located on the side of a first order dendrite (Fig. 1*A* and *B*). The stimulating pipette was placed at a distance of approximately 1 μm from an FM4-64-labelled terminal (Fig. 1*A*–*C*), and an isolated stimulator delivered short depolarising pulses. The following precautions ensured that only one bouton was activated at a time (Kirischuk *et al.* 1999*b*). The selected bouton was always > 2 μm away from its closest FM4-64-labelled neighbour. A small (~1 μm) displacement of the stimulation pipette reversibly abolished both the Ca^{2+} transient and the evoked IPSC. A Ca^{2+} response was detected only in the stimulated boutons.

In the presence of tetrodotoxin (TTX) and antagonists of ionotropic glutamate receptors, the focal stimulation of an individual bouton resulted in a postsynaptic chloride current. The GABAergic nature of the synaptic response was identified by its sensitivity to bicuculline (10 μM), slow time course and reversal at the chloride equilibrium potential (not illustrated). We have shown previously that a 2 ms, 2 μA pulse induces a $[Ca^{2+}]_{pre}$ elevation that is similar to the Ca^{2+} increase caused by an action potential (Kirischuk *et al.* 2002). Therefore, a 2 ms, 2 μA pulse was selected as the standard single-terminal stimulus for all experiments, unless otherwise stated. The period between successive trains of stimuli was at least 1 min.

Selection of stimulation protocol

A stimulation protocol must satisfy the following criteria: (1) it should not modify the postsynaptic cell and (2) it should lead to conditions at which both asynchronous release and $[Ca^{2+}]_{pre}$ remain at quasi-stationary levels. Steady-state conditions could be reached by applying a high-frequency stimulation (Ravin *et al.* 1997) or by using local application of elevated extracellular KCl or ionomycin (Angleson & Betz, 2001). Both approaches have advantages and disadvantages. The efficacy of individual stimuli may fluctuate during a high-frequency train, increasing the

$[Ca^{2+}]_{pre}$ variability. Application of a Ca^{2+} ionophore-containing or hyperkalaemic solution appears to provide a reliable way to elicit steady-state $[Ca^{2+}]_{pre}$ elevations, but it affects the postsynaptic cell, inducing, for instance, a postsynaptic $[Ca^{2+}]$ elevation. In contrast, local electrical stimulation only slightly affects postsynaptic $[Ca^{2+}]$ (Kirischuk *et al.* 1999*b*) and does not activate any significant voltage-dependent postsynaptic conductance (results from three experiments performed in Ca^{2+}-free solution, data not shown). As $GABA_A$ receptors were reported to be sensitive to intracellular $[Ca^{2+}]$ (Inoue *et al.* 1986), we selected local electrical stimulation to induce presynaptic Ca^{2+} influx in individual boutons (but also see Discussion).

Analysis of synchronous, asynchronous and delayed release

Figure 1*D* shows a presynaptic Ca^{2+} transient and a corresponding trace of the postsynaptic chloride current in response to a train of 20 pulses at 50 Hz. Repetitive stimulation causes a compound postsynaptic response. IPSCs that peak within a 3 ms interval following the end of a stimulus pulse will be referred to as synchronous, evoked IPSCs (eIPSCs). All other events during a train will be referred to as asynchronous IPSCs (aIPSCs). IPSCs that were generated after the termination of stimulation will be referred to as delayed IPSCs (dIPSCs). As miniature IPSC (mIPSC) frequencies are quite low ($< 0.5\ s^{-1}$) in these low-density cultures, a possible contribution of mIPSCs stemming from other contacts was ignored.

To make the values obtained from different boutons comparable, eIPSCs were normalised to the mean amplitude of delayed IPSCs (dIPSC) induced at the same synapse (Fig. 1*E*). The mean amplitude of dIPSCs varied from cell to cell (ranging from 12 to 43 pA). The value of normalised eIPSC amplitude was used as an estimate of the number of released vesicles per stimulus (Schneggenburger *et al.* 1999).

The delayed response (DR) was defined as the area under a current trace calculated over the first 3 s after the termination of stimulation. The asynchronous response was defined as the average charge transfer per second calculated over the second half of the stimulation period (for a more precise definition see Results). Stimulus-related capacitance artefacts exhibited a decay time constant of about 1 ms. Therefore, to minimise contamination of the measured parameters by stimulation artefacts, the first 5 ms after the onset of a pulse was excluded from analysis. For each cell, the average dIPSC charge transfer was calculated using well separated individual dIPSCs (Fig. 1*D* and *E*) that had an amplitude close to the mean dIPSC amplitude (Fig. 1*D*, inset). The distribution of dIPSC charge was almost

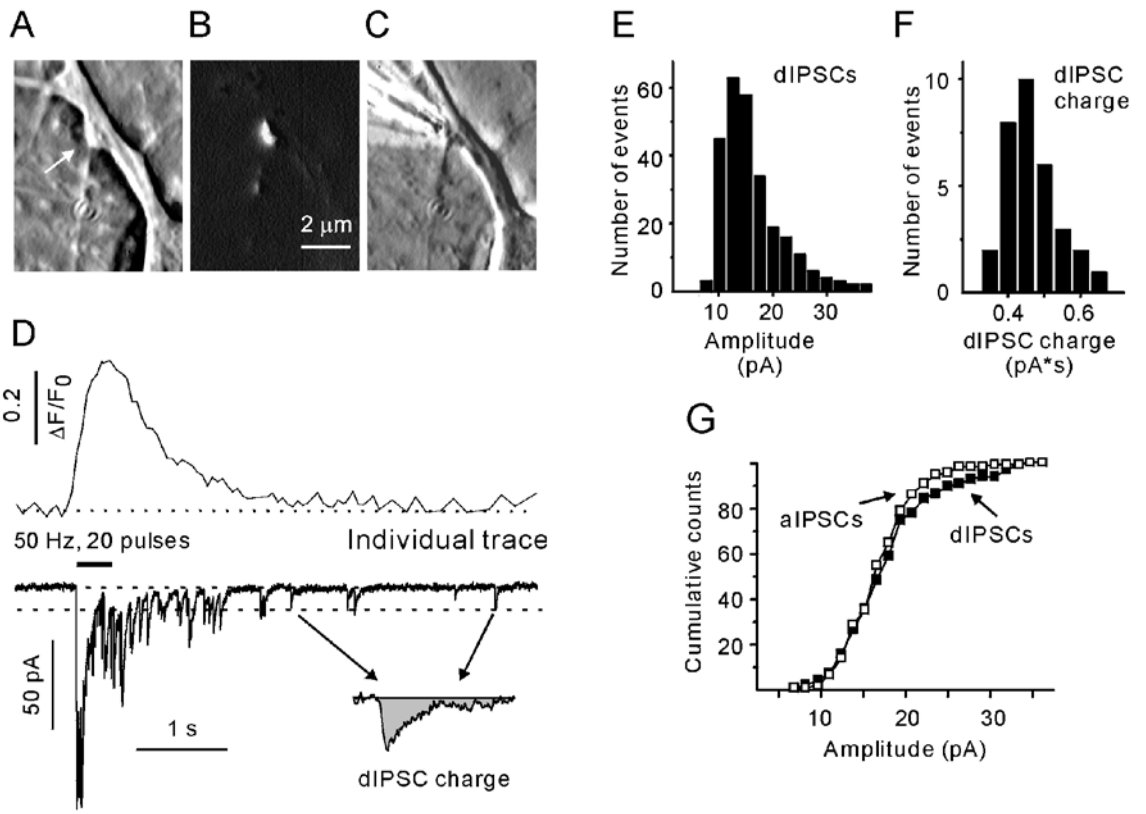

Figure 1. Simultaneous recording of presynaptic Ca^{2+} ($[Ca^{2+}]_{pre}$) transients and inhibitory postsynaptic currents

Phase contrast (*A*) and FM4-64 images (*B*) of a single terminal (arrow). *C*, phase contrast image showing a stimulation pipette in close proximity to a terminal. *D*, single $[Ca^{2+}]_{pre}$ transient and postsynaptic response induced by focal stimulation of a bouton with 20 standard pulses at 50 Hz. The dotted line at the current traces indicate the average amplitude of delayed IPCSs (dIPSCs). The origin of the arrows corresponds to dIPSCs selected for the calculation of dIPSC charge transfer (inset). *E* and *F*, amplitude histograms of dIPSCs (*E*) and dIPSC charge transfer (*F*). *G*, cumulative probability histograms of dIPSCs (filled) and asynchronous IPSCs (aIPSCs; open symbols). All data were obtained from the same synapse.

Gaussian (Fig. 1*F*). There was no significant difference between the mean amplitudes of aIPSCs and dIPSCs (Fig. 1*G*, $n = 6$). The separation of dIPSCs and aIPSCs was made according to the time of their appearance and does not imply that different processes govern the respective release events. To make asynchronous and delayed responses independent of the kinetic properties of IPSCs, both parameters were normalised to the mean dIPSC charge obtained from the same postsynaptic cell. It should be noted that the normalised asynchronous response has the dimension 's^{-1}', and will be referred to as the asynchronous release rate (ARR).

Superfusion

All experiments were performed at room temperature (23–25 °C). A slow superfusion system with a flow rate of 0.5 ml min^{-1} was used. To test the effect of Ca^{2+}-free or Sr^{2+}-containing solution, a glass superfusion pipette (40 μm tip diameter) was placed at a distance of about 50 μm. The Ca^{2+}-free solution contained 2.5 mM $MgCl_2$, no added Ca^{2+} and no EGTA. In Sr^{2+}-containing solution, Ca^{2+} was replaced by Sr^{2+} at equimolar concentration. TTX (1 μM) was added to prevent action potential generation. DL-2-Amino-5-phosphonopentanoic acid (50 μM) and 6,7-dinitroquinoxaline-2,3-dione (10 μM) were added to prevent glutamatergic synaptic transmission. Magnesium Green-AM, Oregon Green BAPTA 488-5N-AM and FM4-64 were obtained from Molecular Probes (Eugene, OR, USA). All other chemicals were from Sigma-Aldrich (Deisenhofen, Germany).

Data analysis and statistics

IPSCs were analysed using the software PeakCount V2.02 (C. Henneberger, Berlin, Germany). The software employed a derivative threshold-crossing algorithm to detect IPSCs. Each automatically detected event was displayed that allowed visual inspection. Rise times and decay time (a single exponential fit) constants of individual IPSCs were calculated. When quantal events overlapped, their decays were obscured and, therefore, respective dIPSCs were not analysed. All results are presented as means ± S.E.M., with n indicating the number of boutons tested. The error bars in all figures indicate S.E.M. All comparisons between means were tested for significance using Student's unpaired t test, unless otherwise stated.

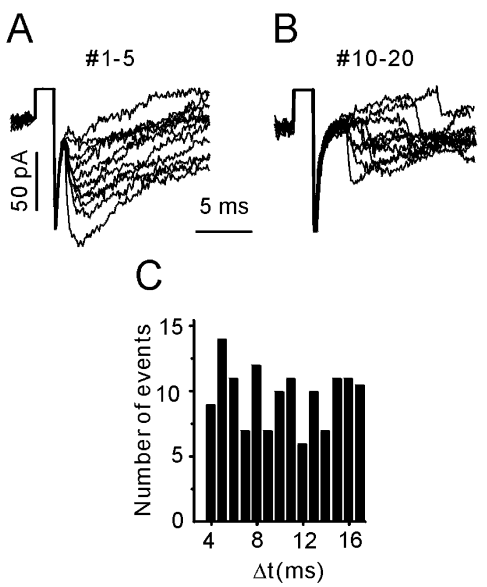

Figure 2. Desynchronisation of neurotransmitter release during a train of stimuli

A and *B*, examples of IPSCs during a 50 Hz train. IPSCs after each stimulus were aligned to the onset of the stimulation artefact. Comparing responses to stimuli 1–5 (*A*) and 10–20 (*B*) reveals asynchrony in *B*. *C*, latency distribution of aIPSCs for stimuli 10–20.

RESULTS

To examine the temporal relationship between IPSC occurrence and electrical stimulation, we applied trains of 20 pulses at 50 Hz and aligned the responses to the onset of each stimulus. Figure 2*A* and *B* shows that the IPSC patterns were quite different during the first five and the last 10 stimulation intervals. Early in the train, IPSCs peaked within the first 3 ms after the termination of stimulus, reflecting the predominantly synchronous mode of release. Later in the train, IPSCs occurred at almost any time (Fig. 2*B* and *C*), reflecting the predominantly asynchronous mode of release.

Dynamics of asynchronous release

Next we wanted to determine the conditions under which the asynchronous mode predominates. As generation of asynchronous IPSCs was paralleled by an augmentation of delayed release (Jensen *et al.* 2000; Lu & Trussell, 2000), pulse trains of increasing duration (3, 5, 7, 10, 15 and 20 stimuli) were delivered to a terminal at 20, 50 (Fig. 3*A*) and 100 Hz, and the DR was calculated. Figure 3*B* shows that at all tested frequencies, the DR reached a plateau after 10 pulses. We conclude that the DR is fully developed after 10–15 stimuli.

Is the above conclusion also valid for the asynchronous release during the train? The impact of asynchronous release was assessed in the following way. We assumed that after each stimulus, eIPSCs rose instantaneously and decayed with a typical single exponential time constant. The latter was determined by a single exponential fitting of the decay phase of pretetanic eIPSCs. Using the typical eIPSC waveform as a template and considering the amplitudes of individual eIPSCs during the train (Fig. 3*C*), the compound evoked response was constructed by adding the contribution from each consecutive eIPSC. The reconstructed eIPSC response was integrated (Microsoft Excel 97), providing the synchronous charge transfer. The difference between the total (observed) and stimulus-locked (constructed) current integrals represents the charge transfer attributed to asynchronous release. During a 50 Hz train, the impact of synchronous release approached zero and asynchronous release reached a plateau with a lag of about 10 pulses (Fig. 3*D*). Similar results were obtained for all frequencies (> 10 Hz) tested (data not shown). In this regard asynchronous release behaves like delayed release. We can conclude that the full shift from the synchronous to the asynchronous mode of transmission is accomplished after 10 pulses

Dependence of asynchronous release on stimulation frequency

Figure 4*A* shows postsynaptic responses elicited with 80 pulse trains delivered to a terminal at increasing rates (20, 50 and 100 Hz). The asynchronous response was defined as the average normalised charge transfer rate calculated over the second half of the stimulation train (40 pulses). The ARR varied dramatically between terminals (Fig. 4*B*). For example, the ARR ranged from 4 to 167 s^{-1} ($n = 19$) when activated with 100 Hz trains. The observed inter-bouton heterogeneity of ARR could reflect the variability in the number of docking/release sites available for presynaptic vesicles. Indeed, ARR normalisation to the ARR elicited with 100 Hz trains revealed that its dependence on the stimulation frequency was quite similar in different terminals (Fig. 4*C*). A strong frequency dependence of the ARR was observed between 10 and 50 Hz. A further increase of the stimulation frequency induced little ARR increment.

Normalisation of ARRs

In principle, the ARR should be dependent on at least two parameters: the number of release sites available for asynchronous release and the rate of vesicle recruitment. We can assume that the former is not dependent on $[Ca^{2+}]_{pre}$ (see below). Therefore, to study the Ca^{2+} dependence of asynchronous release, it is preferable to normalise the obtained ARR values to the number of docking/release sites (N). As N is difficult to measure directly, the size of the RRP has been used to obtain an approximate mean value of N. Repetitive stimulation induces a strong depression of eIPSC amplitudes. Assuming that this depression is largely caused by a transient decrease in the number of readily releasable quanta, it is possible to estimate the RRP on the basis of cumulative eIPSC amplitudes (Schneggenburger *et al.* 1999; Kirischuk & Grantyn, 2000; Lu & Trussell, 2000). Cumulative eIPSC amplitudes were plotted *versus* stimulus number (Fig. 5*A* and *B*). After 10 pulses, the cumulative eIPSCs reached a steady state, as indicated by the linear slope

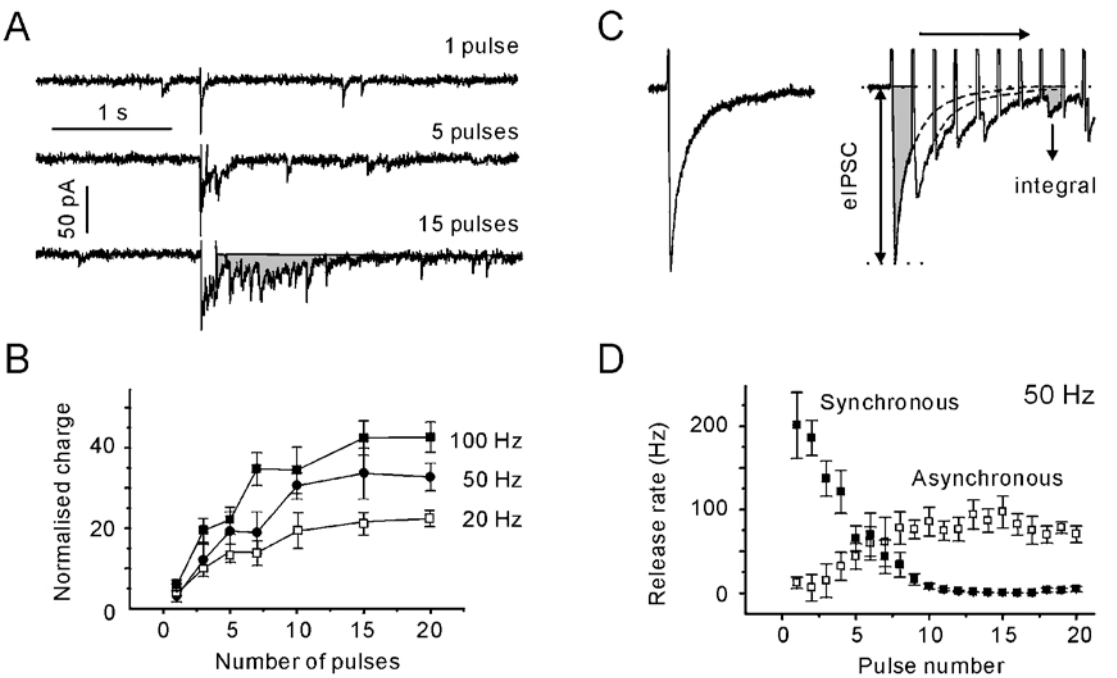

Figure 3. Transition into an asynchronous mode of transmission requires 10 pulses

A, postsynaptic responses elicited with a single pulse and with 50 Hz trains of 5 and 15 pulses. The shaded area represents the delayed response. *B*, dependence of normalised charge transferred after the termination of stimulation on the number of pulses in a train. The delayed response was normalised to the mean charge of the dIPSCs. Note that regardless of the stimulation frequency, the transferred charge reaches a plateau after 10 stimuli. All data points are averages from five synapses. *C*, individual synchronous, evoked IPSC (eIPSC) and IPSCs evoked with a 50 Hz train. eIPSCs were assumed to decay with a typical single exponential time constant. The latter was determined by a single exponential fitting of the decay phase of pretetanic eIPSCs. eIPSCs were constructed using the eIPSC waveform as a template (dotted lines). The total evoked response was constructed by adding the contribution from each eIPSC. The reconstructed eIPSC response was integrated to obtain the synchronous charge transfer. The difference between the observed (shaded areas) and constructed current integrals represents the charge transferred by the asynchronous release. *D*, synchronous and asynchronous release rates during a 50 Hz stimulation. The release rates were obtained by dividing the synchronous/asynchronous charge per second by the mean charge of the dIPSC. Data points are averages from five synapses. Note that the frequency of asynchronous release reached a steady state after 10 pulses.

dependency of the cumulative eIPSC amplitude on the pulse number. Assuming that the linear component reflects vesicle recycling, back-extrapolation to the start of the train gives an estimate for the cumulative eIPSC amplitude in the absence of pool replenishment. If the above approach is correct, the estimate of the RRP must be independent of the stimulation frequency. Figure 5*C* shows that this was the case. The RRP was estimated to contain 6.3 ± 0.8, 6.7 ± 0.9, 6.4 ± 0.8 and 6.2 ± 0.7 vesicles when stimulated at 10, 20, 50 and 100 Hz, respectively ($n = 7$, $P > 0.1$, Student's paired t test).

The use of the RRP as a normalising factor for the ARR would be precluded if synchronously and asynchronously released vesicles originated from different pools. This could be tested. Replacement of extracellular Ca^{2+} by Sr^{2+} was shown to result in a significant suppression of the stimulus-locked postsynaptic response, while the contribution of delayed postsynaptic responses increases (Dodge *et al.* 1969; Mellow *et al.* 1982; Augustine & Eckert, 1984; Goda & Stevens, 1994; Rumpel & Behrends, 1999; Xu-Friedman & Regehr, 2000). If phasic and asynchronous release were mediated by vesicles from different pools, replacement of Ca^{2+} by Sr^{2+} should lead to an increase in the ARR. This was not the case. Phasic release was indeed strongly suppressed in Sr^{2+}-containing solution, but the ARR was not affected (Fig. 5*D*). For example, if stimulated at 50 Hz, ARRs were 15 ± 4 and 16 ± 3 s^{-1} in Ca^{2+}- and Sr^{2+}-containing solution, respectively ($P > 0.1$, $n = 6$, Students's paired t test). We conclude that ARR could be normalised to the RRP estimate from the same bouton, thereby correcting for the pool size variability between terminals.

$[Ca^{2+}]_{pre}$ responses

$[Ca^{2+}]_{pre}$ transients were measured during trains of constant frequency (10, 20, 50 and 100 Hz). $[Ca^{2+}]_{pre}$ rapidly reached a steady state (after about 20 pulses) and then fluctuated around a plateau level that depended on the stimulation frequency (Fig. 6*A*). As the acquisition rate was one image per 50 ms and the number of pulses in a train was set to 80, only 16 experimental points were acquired during a 100 Hz train. To exclude that the amplitudes of $[Ca^{2+}]_{pre}$ transients were underestimated, trains of 200 pulses were tested as well. No additional $[Ca^{2+}]_{pre}$ increase was observed ($n = 3$, data not shown). Therefore, a plateau level of $[Ca^{2+}]_{pre}$ was defined as the average fluorescence signal during the last half of the stimulation trains (40 pulses). The amplitude of train-induced $[Ca^{2+}]_{pre}$ elevation varied dramatically between terminals (Fig. 6*B*). The observed heterogeneity of $[Ca^{2+}]_{pre}$ transients presumably reflects the interbouton variability of single pulse-induced $[Ca^{2+}]_{pre}$ transients (Kirischuk & Grantyn, 2002). Indeed, normalisation to the amplitude of the $[Ca^{2+}]_{pre}$ transient elicited by a 100 Hz train revealed that the dependence of $[Ca^{2+}]_{pre}$ increase on the stimulation frequency was quite similar in different terminals (Fig. 6*C*). A 10 Hz train only induced a slight $[Ca^{2+}]_{pre}$ elevation. Stimulation frequencies of 20 or 50 Hz resulted in a substantially higher $[Ca^{2+}]_{pre}$ rise, but further frequency increase produced little additional increment in the $[Ca^{2+}]_{pre}$ responses.

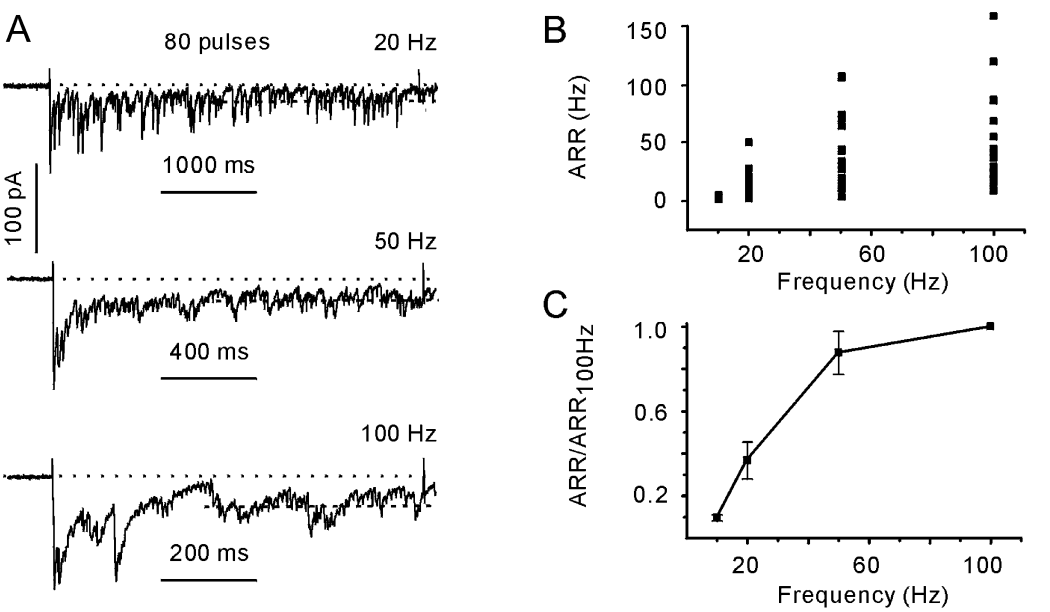

Figure 4. Dependence of the asynchronous release rate (ARR) on stimulation frequency

A, examples of IPSCs evoked with 80 pulses delivered at 20, 50 and 100 Hz. Data from the same cell. *B*, interbouton variability of ARRs. Data obtained from 19 presynaptic terminals. *C*, dependence of the ARR on stimulation frequency. For each cell, values of ARRs were normalised to the ARR elicited with a 100 Hz train. Same data set as in *B*.

The affinity of MG for Ca^{2+} is reported to be about 6 μM (Molecular Probes catalogue). The $[Ca^{2+}]_{pre}$ elevation in response to a long, high-frequency train can potentially saturate the Ca^{2+} indicator. To examine this possibility, the cultures were loaded with another Ca^{2+} probe, Oregon Green 488 BAPTA-5N (OGB-5N). The latter is reported to have an affinity for Ca^{2+} of 20 μM (Molecular Probes catalogue) or even 32 μM (DiGregorio & Vergara, 1997). Figure 6*C* shows that the relationship between the peak amplitude of $[Ca^{2+}]_{pre}$ and the stimulation frequency was not dependent on the indicator. In five experiments, a control pulse train was followed by a test train of stronger (4 μA) pulses. The $[Ca^{2+}]_{pre}$ elevations elicited with a train of strong shocks were irreversible, presumably reflecting bouton damage (Fig. 6*D*). The mean increase in the fluorescence signal was 3.5 ± 0.5 (range 3–4.5), which is much higher than the maximal experimental values. Next, we performed *in vitro* calibration of the MG signals. The fluorescence signals were measured using droplets of solutions containing different Ca^{2+} concentrations (0–39 μM, Calibration Buffer Kit 2, Molecular Probes) and supplemented with 10 μM of MG-K_5 (Fig. 6*E*). The maximum : minimum fluorescence ratio for MG *in vitro* was 7.7. We conclude that under given experimental conditions, MG is still far from saturation and, regardless of the stimulation frequency, $[Ca^{2+}]_{pre}$ levels reach a steady state during trains of 80 pulses.

In the present study, $[Ca^{2+}]_{pre}$ was measured by means of the non-ratiometric Ca^{2+}-sensitive indicator MG. Consequently, a linear dependence of obtained fluorescence changes ($\Delta F/F_0$) and $[Ca^{2+}]$ is of particular importance, while any non-linearity will, in turn, have an effect on the ARR–$[Ca^{2+}]_{pre}$ relationship. The power function fitting of the lower part ($\Delta F/F_0$ from 0 to 2) of the calibration curve had an exponent of 1.1 ± 0.1 (Fig. 6*E*, inset). Thus, the relationship was indeed close to linear for the observed fluorescence changes.

The ARR exhibits a third-power function dependence on $[Ca^{2+}]_{pre}$

First, the relationship between ARR and $[Ca^{2+}]_{pre}$ was investigated at individual boutons. The ARR increased in a non-linear fashion as $[Ca^{2+}]_{pre}$ rose (Fig. 7*A*). The power function fitting the data points had an exponent of 2.8 ± 0.5 (range 2.1–3.9, n = 13). Next, ARRs were normalised to the RRPs. The power function fitting the pooled data set revealed an exponent of 2.6 ± 0.3 (Fig. 7*B*), which is close to the mean value obtained from individual boutons (i.e. before normalisation to the RRPs). This result represents an additional piece of evidence supporting the use of the RRP value for the normalisation of the ARR.

As delayed release is driven by residual $[Ca^{2+}]_{pre}$ (Katz & Miledi, 1967; Delaney & Tank, 1994; Lu & Trussell, 2000), we investigated its Ca^{2+} dependence. Figure 7*C* shows that delayed activity terminated much faster than the $[Ca^{2+}]_{pre}$

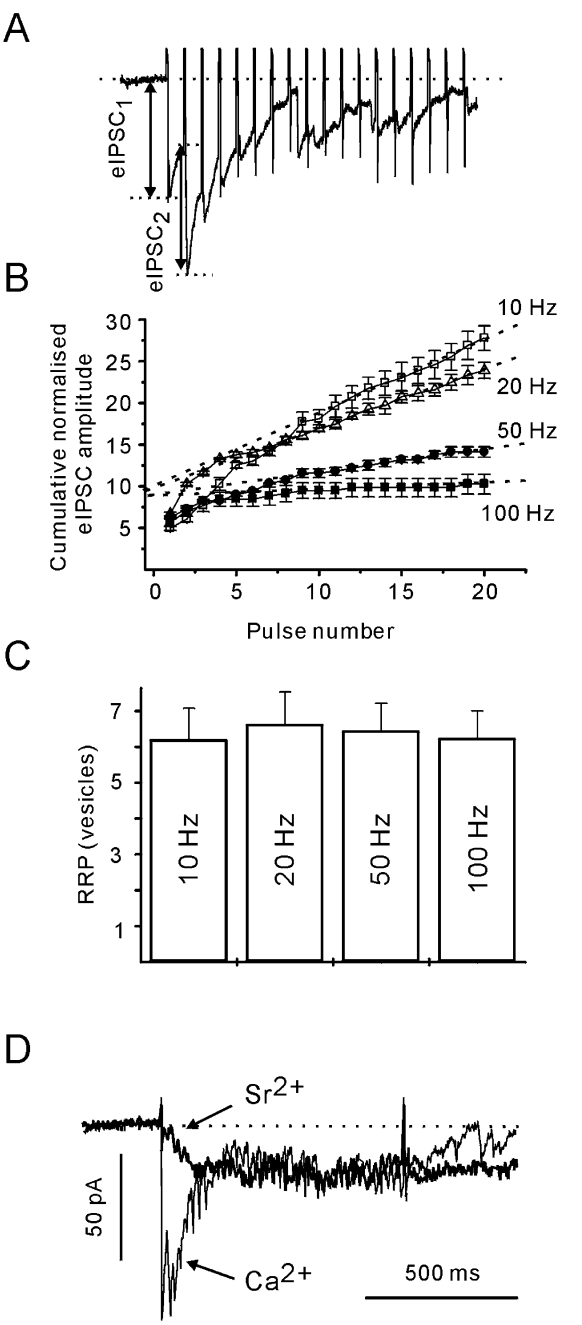

Figure 5. Estimation of the size of the readily releasable pool (RRP) at individual boutons

A, postsynaptic responses to first 15 stimuli of a 50 Hz train. *B*, peak eIPSC amplitude values were summed to determine the cumulative eIPSC amplitude during trains of different frequencies. Evoked IPSCs were normalised to the mean dIPSC amplitude. Each data point is an average of three trials. Data from the same cell. Data points during a steady state phase (from the 10th to the 20th pulse) were fitted by linear regression (dotted lines), and back-extrapolated to time 0. The intersects provide an estimate of the number of available vesicles. *C*, RRP size does not depend on stimulation frequency. Shown data are from seven cells. *D*, the ARR is not modified by the substitution of Sr^{2+} (thick line) for extracellular Ca^{2+} (thin line). Each trace is an average of five responses.

transients. The decay phase of delayed release and $[Ca^{2+}]_{pre}$ was fitted with a single exponent. The difference between the time constants was highly significant ($P < 0.0001$, 12 cells, Student's paired t test), but they were strongly correlated ($r = 0.68$, Fig. 7*D*), consistent with the notion that residual $[Ca^{2+}]_{pre}$ underlies the delayed release. The slope of the linear regression line was 2.2. Assuming a power function dependence of delayed release on $[Ca^{2+}]_{pre}$, this result means that the respective exponent equals 2.2. Although the high-power law relationship between the delayed release and $[Ca^{2+}]_{pre}$ under non-stationary conditions should be considered with caution (Atluri & Regehr, 1998), we may tentatively conclude that this dependence can be described as a power function with an exponent larger than 2.

Estimation of the affinity of the Ca^{2+} sensor for asynchronous release

The lack of clear saturation in the Ca^{2+} dependence of ARR prohibits a direct determination of the affinity of Ca^{2+} sensors for asynchronous release. However, an estimate of the Ca^{2+} sensitivity of asynchronous release can be obtained using the following approach. The Hill equation for the Ca^{2+} dependence of synaptic responses (modified eqn (2) from Dodge & Rahamimoff, 1967):

$$\mathrm{ARR} = \mathrm{ARR}_{max}(\Delta F/F_0)^n/(K_{ar} + \Delta F/F_0)^n, \quad (1)$$

can be rearranged to give:

$$\frac{1}{(\mathrm{ARR})^{1/n}} = \left(\frac{K_{ar}}{(\mathrm{ARR}_{max})^{1/n}}\right)\left(\frac{1}{\Delta F/F_0}\right) + \frac{1}{(\mathrm{ARR}_{max})^{1/n}}, \quad (2)$$

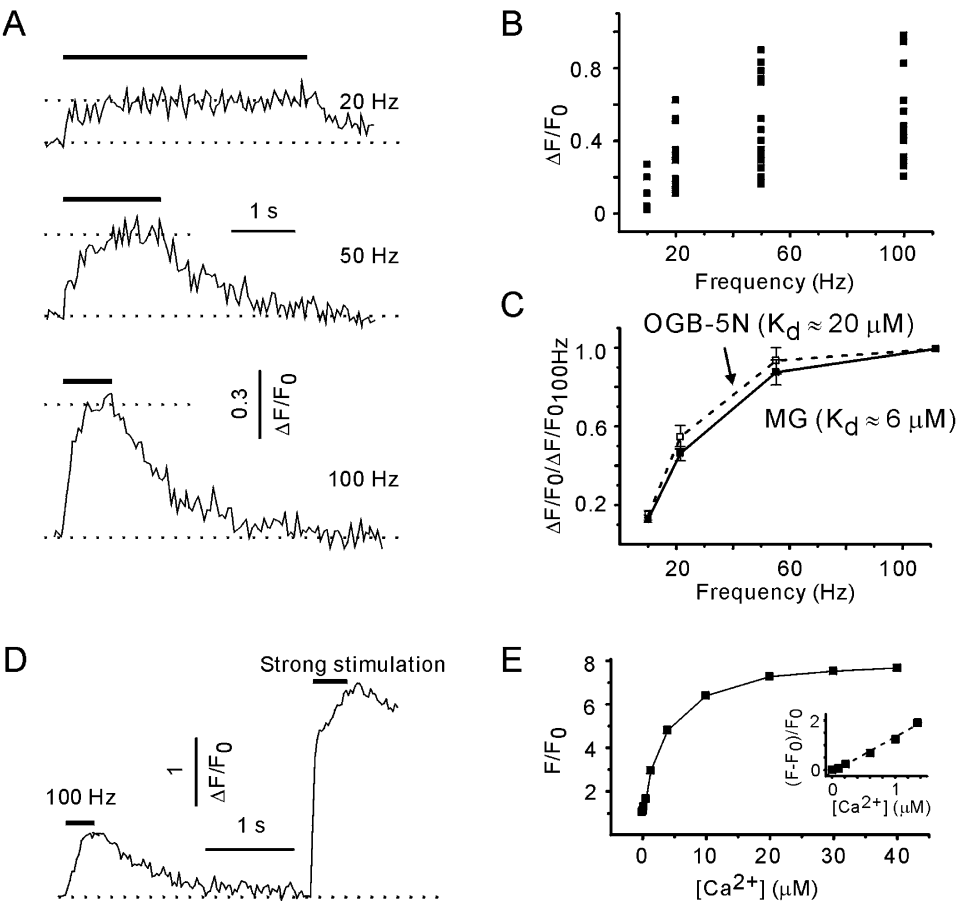

Figure 6. $[Ca^{2+}]_{pre}$ responses exhibit a non-linear dependency on stimulation frequency

A, examples of $[Ca^{2+}]_{pre}$ transients induced with 20, 50 and 100 Hz trains. Data from the same synapse. $[Ca^{2+}]_{pre}$ transients were visualised using Magnesium Green (MG). *B*, interbouton variability of $[Ca^{2+}]_{pre}$ responses. Data obtained from 13 presynaptic terminals. *C*, dependence of $[Ca^{2+}]_{pre}$ plateau levels on the stimulation frequency. For each synapse, $[Ca^{2+}]_{pre}$ responses were normalised to the peak amplitude of $[Ca^{2+}]_{pre}$ at 100 Hz. Same data as in *B*. Oregon Green 488 BAPTA-5N (OGB-5N), a Ca^{2+} probe with lower affinity, did not modify the frequency dependence (five boutons). *D*, a train of stronger pulses induced a much larger (although irreversible) elevation of presynaptic fluorescence than a 100 Hz train with standard pulses. *E*, calibration curve for MG. Calibration was performed *in vitro* using droplets of solutions containing 10 μM MG-K_5 and variable Ca^{2+} concentrations. F_0 is the fluorescence of MG in Ca^{2+}-free solution. Inset, expansion of the lower part of the curve with a modified y-axis. Note the linear relationship between $\Delta F/F_0$ and $[Ca^{2+}]$ (dotted line).

where ARR_{max} is the maximal possible frequency of asynchronous release, n is the Hill coefficient, and K_{ar} is the half-effective Ca^{2+} concentration for asynchronous release (Ravin *et al.* 1997). In this case, however, K_{ar} is a dimensionless parameter, because MG is a non-ratiometric Ca^{2+}-sensitive probe. The $1/(ARR)^{1/n}$ *vs.* $1/(\Delta F/F_0)$ plot represents a straight line with a slope of $K_{ar}/(ARR_{max})^{1/n}$ and a y-axis intercept of $1/(ARR_{max})^{1/n}$ (Ravin *et al.* 1997).

Based on the present results, the Hill coefficient was set to 3. Figure 7*E* shows the results from two boutons. The average K_{ar} and ARR_{max} values were 0.6 ± 0.1 s^{-1} (range 0.36–1.1 s^{-1}) and 43 ± 13 s^{-1} (range 17–86 s^{-1}, $n = 7$). The pooled data from 19 boutons were best fitted with 0.72 and 63 s^{-1} for K_{ar} and ARR_{max}, respectively (Fig. 7*F*). Two data points with fluorescence changes less than 0.05 (about the instrumental noise level) were excluded from this analysis. It is worth mentioning that amplitude of $[Ca^{2+}]_{pre}$ transients induced by 100 Hz stimulation was between 0.12 and 0.95: These values are close to the K_{ar} estimate. This result allows us to suggest that the Ca^{2+} sensor for asynchronous release is not saturated, at least under the conditions used in this study.

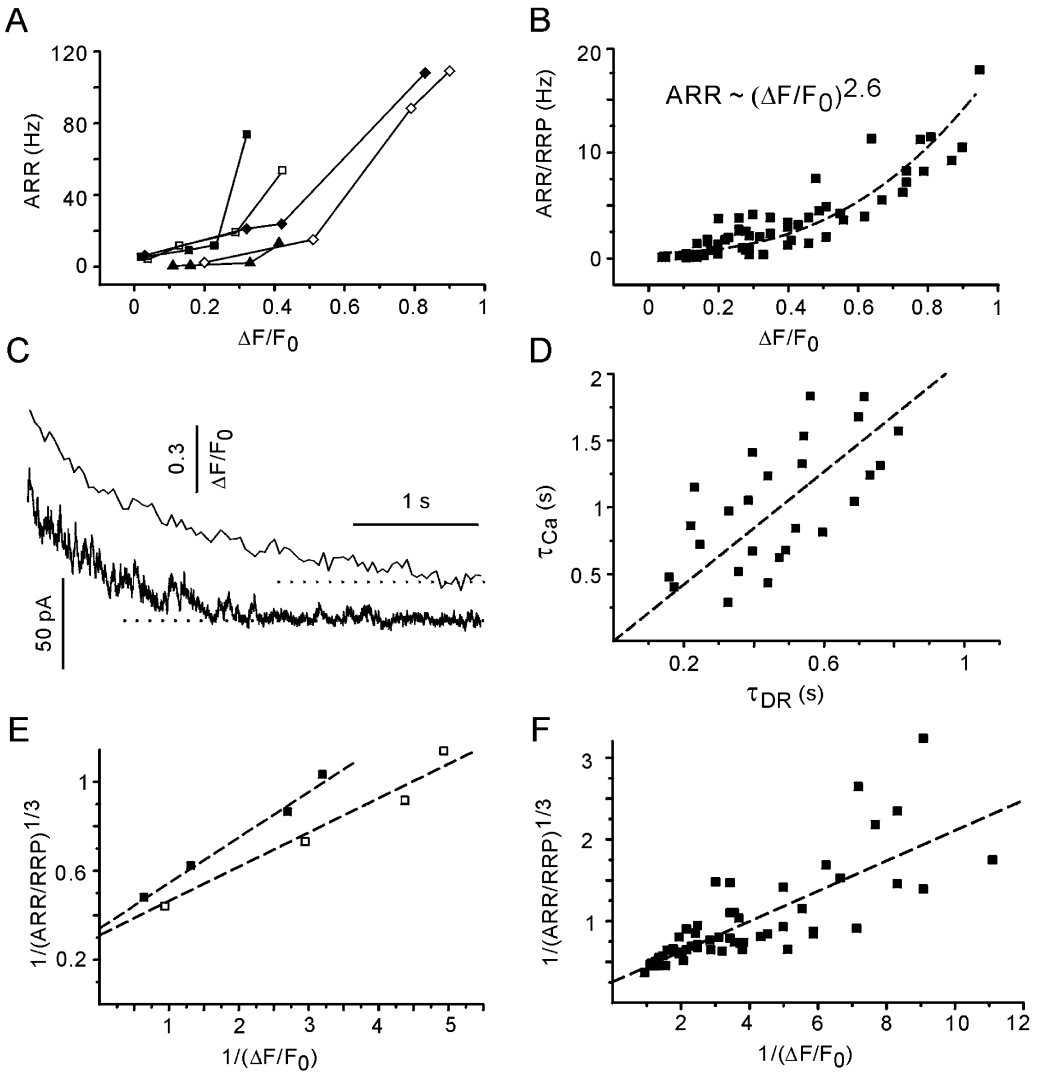

Figure 7. Relationship between $[Ca^{2+}]_{pre}$ and ARR

A, dependence of ARR on the peak amplitude of $[Ca^{2+}]_{pre}$ elevation. Different symbols represent data obtained from different boutons. *B*, ARR as a function of $[Ca^{2+}]_{pre}$ (pooled results, 19 boutons). ARRs were normalised to the corresponding RRP size. The dashed line represents the power function fit. *C*, the delayed response decays faster than the $[Ca^{2+}]_{pre}$ transient. The $[Ca^{2+}]_{pre}$ trace was shifted up for clarity. Dotted lines represent the baselines for IPSCs and $[Ca^{2+}]_{pre}$. Traces represent the average of five recordings. *D*, correlation between decay time constants of delayed response (τ_{DR}) and $[Ca^{2+}]_{pre}$. Data from 12 boutons. The line represents a linear regression fit. *E*, estimation of the maximal ARR (ARR_{max}) and the affinity of the Ca^{2+} sensor (K_{AR}). Data obtained from two boutons (filled and open squares). Linear regression fits (lines) are based on eqn (2). *F*, pooled data from 19 boutons. The dashed line is computed according to eqn (2).

DISCUSSION

We have studied the Ca^{2+} dependence of asynchronous release at single GABAergic boutons during repetitive stimulation. Delayed synaptic responses were observed when individual inhibitory boutons were activated at frequencies higher than 10 Hz. During the trains, the stimulus-locked quantal release drastically declined, and vesicles were liberated asynchronously. The asynchronous mode of transmission became dominant after 10–15 pulses. These values are close to those reported for hippocampal cells (Jensen *et al.* 2000) and nMag neurones in the avian cochlear nucleus (Fig. 2 in Lu & Trussell, 2000). In those studies, synaptic connections were activated using action potentials. The good agreement between data obtained with action potential- or pulse-induced release lends further support to our claim that direct electrical stimulation of small terminals can be used to study particular aspects of synaptic transmission.

Phasic and asynchronous release use the same set of release sites

Because of the bleaching of the Ca^{2+}-sensitive probe, we were only able to collect four to five experimental points per bouton. This number is too small to allow a detailed analysis of the $[Ca^{2+}]_{pre}$–ARR relationship. To circumvent this problem, a pooled data set from 13 boutons was composed by normalising the data to the size of RRP (Schneggenburger *et al.* 1999). This normalisation was based on the assumption that the size of the RRP determines the number of release sites available for asynchronous release (Lu & Trussell, 2000; Hagler & Goda, 2001). However, the question as to whether phasic and asynchronous release originate from the same pool has not yet been resolved. Based on the different sensitivity of phasic and asynchronous release to Sr^{2+}, delayed release was suggested to result from the action of residual Ca^{2+} on a specific high-affinity sensor (Goda & Stevens, 1994; Gad *et al.* 1998; Zucker, 1999), presumably synaptotagmin III (Li *et al.* 1995). However, later investigations showed that less efficient buffering and extrusion of Sr^{2+} may underlie the potentiating effect of Sr^{2+} on asynchronous release (Rumpel & Behrends, 1999; Xu-Friedman & Regehr, 2000). In line with the latter reports, replacement of extracellular Ca^{2+} by Sr^{2+} had no effect on the steady-state level of ARR in the present study. This result allows us to suggest that during repetitive stimulation, Ca^{2+} and Sr^{2+} activate the same pool of vesicles. But would it be correct to refer to that pool as RRP? Some indirect results favour the idea. Firstly, the RRP size was not dependent on the stimulation frequency and, as a consequence, on the $[Ca^{2+}]_{pre}$ level. Although one cannot completely exclude the effect of unreliability of extracellular electrical stimulation, this result supports the idea that high $[Ca^{2+}]_{pre}$ does not activate additional release sites. Secondly, if distinct vesicle pools served the stimulus-locked and asynchronous modes of release, ARR normalisation to the RRP should affect the $[Ca^{2+}]_{pre}$–ARR relationship for the pooled data. However, the Hill coefficients calculated from individual and normalised pooled data sets were similar (2.8 and 2.6, respectively), while the Hill coefficient estimated from the non-normalised pooled data (1.4) differed significantly. Thus, although direct evidence is still missing, our data are consistent with the assumption that phasic and asynchronous release both originate from the same pool of vesicles in these GABAergic synapses.

Consequently, the normalised ARR is a quantitative parameter for one release site and reflects the mean time required for a vesicle to be recruited and released. The observed maximal release rate per vesicle was about 20 s^{-1} (i.e. the cycle time was 50 ms). At chicken calyx synapses, the vesicle recovery time during the 200 Hz trains was calculated to be 40 ms (Lu & Trussell, 2000). Our directly measured value is in good agreement with the theoretical prediction.

The Ca^{2+} sensor for asynchronous release exhibits a high affinity for Ca^{2+}

Direct measurement of the half-effective Ca^{2+} concentration (K_{ar} in our notation) of the Ca^{2+} sensor for asynchronous transmitter release has been carried out in few preparations. The K_{ar} of the neuromuscular junction is reported to be in a range of 2–4 μM in frog (Ravin *et al.* 1997) or about 1 μM in crayfish (Angleson & Betz, 2001). The relatively low Ca^{2+} level requirement of exocytosis has also been shown in rod photoreceptor cells (Rieke & Schwartz, 1996) and in chromaffin cells (Augustine & Neher, 1992).

Our estimate of K_{ar} is 0.7 a.u. K_{ar} can also be estimated by using eqn (1) and the assumed value of ARR_{max}. At calyces of Held, the maximal release rate per vesicle measured after the depletion of RRP is reported to be about 200 s^{-1} (Fig. 4 in Sakaba & Neher, 2001). Therefore, ARR_{max} was varied between 20 (the highest value observed in this study) and 200 s^{-1}. The resulting K_{ar} ranged from 0.3 to 1.1. K_{ar} increased with elevation of the assumed ARR_{max} value. Higher values of the Hill coefficient resulted in lower values of K_{ar}. The K_{ar} range obtained with this method is quite similar to that obtained from fitting the pooled experimental data with eqn (2).

The fact that the Ca^{2+} indicator is far from saturation (Fig. 6*C* and *D*) provides an opportunity to convert fluorescence changes ($\Delta F/F$) to absolute $[Ca^{2+}]$ values using the formula (Jaffe *et al.* 1992):

$$[Ca^{2+}]_i = \frac{[Ca^{2+}]_{rest} + K_D \times (\Delta F/F)/(\Delta F/F)_{max}}{1 - (\Delta F/F)/(\Delta F/F)_{max}}, \qquad (3)$$

where $(\Delta F/F)_{max}$ is the maximal fluorescence change upon saturation, and K_D is the affinity of MG for Ca^{2+}. Suggesting $[Ca^{2+}]_{rest} \ll K_D(\Delta F/F)/(\Delta F/F)_{max}$ and $[Ca^{2+}]_i$, eqn (3) simplifies as:

$$[Ca^{2+}]_i = K_D \frac{(\Delta F/F)/(\Delta F/F)_{max}}{1 - (\Delta F/F)/(\Delta F/F)_{max}}. \quad (4)$$

Taking values of 3.5 (Fig. 6*D*) and 6 μM (Molecular Probes catalogue) for $(\Delta F/F)_{max}$ and K_D, respectively, we obtain a K_{ar} value of 1.5 μM. However, this K_{ar} estimate is dependent on several still unclear conditions. Firstly, it is assumed that there is a linear relationship between $\Delta F/F$ and $[Ca^{2+}]_{pre}$. Although our *in vitro* calibration curve (Fig. 6*E*, inset) supports this assumption, it remains unclear whether this relationship can be extended to the *in vivo* situation. Secondly, the *in vivo* affinity of MG for Ca^{2+} was not determined in the present study. The *in vivo* K_D could be two times higher than *in vitro* (Zhao *et al.* 1996). Therefore, the K_{ar} value obtained here (1.5 μM) cannot be much more than an order estimate for the affinity of the Ca^{2+} sensor. In other words, in these GABAergic terminals the affinity of the Ca^{2+} sensor for asynchronous release should be in the lower micromolar range.

The Ca^{2+} sensor for asynchronous release is most likely not saturated

As the affinity of the Ca^{2+} sensor for asynchronous release is high, it is important to know whether it is saturated during the periods of activity. When the terminals were stimulated in standard solution, the Ca^{2+} dependence of ARR did not exhibit clear saturation. To induce larger $[Ca^{2+}]_{pre}$ transients, two additional experiments were performed. First, terminals were stimulated with 50 Hz trains in control and in high extracellular Ca^{2+} (5 mM) solutions. However, the steady-state levels of $[Ca^{2+}]_{pre}$ were not significantly different in normal and in elevated $[Ca^{2+}]$ ($n = 4$). Consequently, no difference was found between the ARR values in control and elevated Ca^{2+} solutions. The observed ceiling level of $[Ca^{2+}]_{pre}$ presumably reflects the Ca^{2+}-dependent inactivation of Ca^{2+} channels (Kirischuk *et al.* 2002). Therefore, as a next step, we used a Ca^{2+} ionophore, ionomycin, which induces a Ca^{2+}-channel-independent Ca^{2+} influx. Ionomycin (10 μM) was applied to a synaptic terminal very locally, via a stimulation pipette. It caused an increase of $[Ca^{2+}]_{pre}$ to 2.5–3 a.u., and the ARR reached 60–100 s^{-1} ($n = 3$). However, the development of $[Ca^{2+}]_{pre}$ increase in the bouton was rather slow (minutes), and $[Ca^{2+}]_{pre}$ elevations were also detected in neighbouring terminals. Therefore, it is quite possible that the measured ARRs represented the activity of several boutons. Thus, we have to admit than the attempts to show a non-saturation of the Ca^{2+} sensor directly were not successful.

Nevertheless, our data present indirect evidence against the saturation of the Ca^{2+} sensor. First, the ARR–$[Ca^{2+}]_{pre}$ plots for individual boutons or pooled data did not exhibit a plateau (Fig. 7). Second, the measured amplitudes of Ca^{2+} transients were in the same order of magnitude as the affinity of the Ca^{2+} sensor. Although direct measurements are still required to underscore this conclusion, it seems very likely that in these GABAergic terminals the Ca^{2+} sensor for asynchronous transmitter release is not saturated.

Ca^{2+} sensitivity of asynchronous release

Provided the Ca^{2+} sensor for asynchronous release is not saturated, the shape of the Ca^{2+} dependence of asynchronous release gains additional importance. If the relationship is highly supralinear, small fluctuations in presynaptic Ca^{2+} levels should have strong impact on synaptic strength. Both delayed and asynchronous release exhibited a non-linear dependence on the $[Ca^{2+}]_{pre}$ in our preparation. The power function fitting revealed an exponent of 2.2 and 2.8 for delayed and asynchronous release, respectively. It may well be that the smaller exponent for delayed release results from our attempt to link two non-stationary processes: delayed release and decay of $[Ca^{2+}]_{pre}$. The relationship may also contain a time-dependent component, as was suggested for cerebellar synapses (Atluri & Regehr, 1998). We therefore suggest that the exponent of this power function is closer to 3. Interestingly, the cooperativity of Ca^{2+} binding is similar to that previously obtained for stimulus-locked IPSCs (Kirischuk *et al.* 1999*a*). The Ca^{2+} sensor for phasic release has also been reported to be far from saturated (Bollmann *et al.* 2000; Schneggenburger & Neher, 2000). A lack of saturation of the Ca^{2+} sensor and a highly supralinear dependence of release on $[Ca^{2+}]_{pre}$ makes the asynchronous as well as the stimulus-locked response very sensitive to modulatory mechanisms resulting in changes of $[Ca^{2+}]_{pre}$.

Taken together, the present data show that asynchronous release may be a powerful but delicately regulated mechanism that ensures the maintenance of appropriate inhibition when the RRP of vesicles is depleted.

REFERENCES

Angleson JK & Betz WJ (2001). Intraterminal Ca^{2+} and spontaneous transmitter release at the frog neuromuscular junction. *J Neurophysiol* **85**, 287–294.

Atluri PP & Regehr WG (1998). Delayed release of neurotransmitter from cerebellar granule cells. *J Neurosci* **18**, 8214–8227.

Augustine GJ, Adler EM & Charlton MP (1991). The calcium signal for transmitter secretion from presynaptic nerve terminals. *Ann N Y Acad Sci* **635**, 365–381.

Augustine GJ & Eckert R (1984). Divalent cations differentially support transmitter release at the squid giant synapse. *J Physiol* **346**, 257–271.

Augustine GJ & Neher E (1992). Calcium requirements for secretion in bovine chromaffin cells. *J Physiol* **450**, 247–271.

Bollmann JH, Sakmann B & Borst JG (2000). Calcium sensitivity of glutamate release in a calyx-type terminal. *Science* **289**, 953–957.

Cummings DD, Wilcox KS & Dichter MA (1996). Calcium-dependent paired-pulse facilitation of miniature EPSC frequency accompanies depression of EPSCs at hippocampal synapses in culture. *J Neurosci* **16**, 5312–5323.

Delaney KR & Tank DW (1994). A quantitative measurement of the dependence of short-term synaptic enhancement on presynaptic residual calcium. *J Neurosci* **14**, 5885–5902.

Del Castillo J & Katz B (1954). Statistical factors involved in neuromuscular facilitation and depression. *J Physiol* **124**, 574–585.

DiGregorio DA & Vergara JL (1997). Localized detection of action potential-induced presynaptic calcium transients at a *Xenopus* neuromuscular junction. *J Physiol* **505**, 585–592.

Dodge FA Jr, Miledi R & Rahamimoff R (1969). Strontium and quantal release of transmitter at the neuromuscular junction. *J Physiol* **200**, 267–283.

Dodge FA Jr & Rahamimoff R (1967). Co-operative action of calcium ions in transmitter release at the neuromuscular junction. *J Physiol* **193**, 419–432.

Gad H, Low P, Zotova E, Brodin L & Shupliakov O (1998). Dissociation between Ca^{2+}-triggered synaptic vesicle exocytosis and clathrin-mediated endocytosis at a central synapse. *Neuron* **21**, 607–616.

Goda Y & Stevens CF (1994). Two components of transmitter release at a central synapse. *Proc Natl Acad Sci U S A* **91**, 12942–12946.

Hagler DJ Jr & Goda Y (2001). Properties of synchronous and asynchronous release during pulse train depression in cultured hippocampal neurons. *J Neurophysiol* **85**, 2324–2334.

Inoue M, Oomura Y, Yakushiji T & Akaike N (1986). Intracellular calcium ions decrease the affinity of the GABA receptor. *Nature* **324**, 156–158.

Jaffe DB, Johnston D, Lasser-Ross N, Lisman JE, Miyakawa H & Ross WN (1992). The spread of Na^{+} spikes determines the pattern of dendritic Ca^{2+} entry into hippocampal neurons. *Nature* **357**, 244–246.

Jensen K, Lambert JD & Jensen MS (2000). Tetanus-induced asynchronous GABA release in cultured hippocampal neurons. *Brain Res* **880**, 198–201.

Kamiya H & Zucker RS (1994). Residual Ca^{2+} and short-term synaptic plasticity. *Nature* **371**, 603–606.

Katz B (1969). *The Release of Neural Transmission Substances*. Liverpool University Press, Liverpool.

Katz B & Miledi R (1967). The release of acetylcholine from nerve endings by graded electric pulses. *Proc R Soc Lond B Biol Sci* **167**, 23–38.

Kirischuk S, Clements JD & Grantyn R (2002). Presynaptic and postsynaptic mechanisms underlie paired pulse depression at single GABAergic boutons in rat collicular cultures. *J Physiol* **543**, 99–116.

Kirischuk S & Grantyn R (2000). A readily releasable pool of single inhibitory boutons in culture. *Neuroreport* **11**, 3709–3713.

Kirischuk S & Grantyn R (2002). Inter-bouton variability of synaptic strength correlates with heterogeneity of presynaptic Ca^{2+} signals. *J Neurophysiol* **88**, 2172–2176.

Kirischuk S, Veselovsky N & Grantyn R (1999*a*). Relationship between presynaptic calcium transients and postsynaptic currents at single gamma-aminobutyric acid (GABA)ergic boutons. *Proc Natl Acad Sci U S A* **96**, 7520–7525.

Kirischuk S, Veselovsky N & Grantyn R (1999*b*). Single-bouton-mediated synaptic transmission: postsynaptic conductance changes in their relationship with presynaptic calcium signals. *Pflügers Arch* **438**, 716–724.

Li C, Davletov BA & Sudhof TC (1995). Distinct Ca^{2+} and Sr^{2+} binding properties of synaptotagmins. Definition of candidate Ca^{2+} sensors for the fast and slow components of neurotransmitter release. *J Biol Chem* **270**, 24898–24902.

Llinas R, Sugimori M & Silver RB (1995). The concept of calcium concentration microdomains in synaptic transmission. *Neuropharmacology* **34**, 1443–1451.

Lu T & Trussell LO (2000). Inhibitory transmission mediated by asynchronous transmitter release. *Neuron* **26**, 683–694.

Meinrenken CJ, Borst JG & Sakmann B (2002). Calcium secretion coupling at calyx of held governed by nonuniform channel-vesicle topography. *J Neurosci* **22**, 1648–1667.

Mellow AM, Perry BD & Silinsky EM (1982). Effects of calcium and strontium in the process of acetylcholine release from motor nerve endings. *J Physiol* **328**, 547–562.

Neher E (1998). Vesicle pools and Ca^{2+} microdomains: new tools for understanding their roles in neurotransmitter release. *Neuron* **20**, 389–399.

Oleskevich S & Walmsley B (2002). Synaptic transmission in the auditory brainstem of normal and congenitally deaf mice. *J Physiol* **540**, 447–455.

Perouansky M & Grantyn R (1989). Separation of quisqualate- and kainate-selective glutamate receptors in cultured neurons from the rat superior colliculus. *J Neurosci* **9**, 70–80.

Ravin R, Spira ME, Parnas H & Parnas I (1997). Simultaneous measurement of intracellular Ca^{2+} and asynchronous transmitter release from the same crayfish bouton. *J Physiol* **501**, 251–262.

Rieke F & Schwartz EA (1996). Asynchronous transmitter release: control of exocytosis and endocytosis at the salamander rod synapse. *J Physiol* **493**, 1–8.

Rumpel E & Behrends JC (1999). Sr^{2+}-dependent asynchronous evoked transmission at rat striatal inhibitory synapses *in vitro*. *J Physiol* **514**, 447–458.

Sakaba T & Neher E (2001). Quantitative relationship between transmitter release and calcium current at the calyx of Held synapse. *J Neurosci* **21**, 462–476.

Schneggenburger R, Meyer AC & Neher E (1999). Released fraction and total size of a pool of immediately available transmitter quanta at a calyx synapse. *Neuron* **23**, 399–409.

Schneggenburger R & Neher E (2000). Intracellular calcium dependence of transmitter release rates at a fast central synapse. *Nature* **406**, 889–893.

Simon SM & Llinas RR (1985). Compartmentalization of the submembrane calcium activity during calcium influx and its significance in transmitter release. *Biophys J* **48**, 485–498.

Xu-Friedman MA & Regehr WG (2000). Probing fundamental aspects of synaptic transmission with strontium. *J Neurosci* **20**, 4414–4422.

Zhao M, Hollingworth S & Baylor SM (1996). Properties of tri- and tetracarboxylate Ca^{2+} indicators in frog skeletal muscle fibers. *Biophys J* **70**, 896–916.

Zucker RS (1999). Calcium- and activity-dependent synaptic plasticity. *Curr Opin Neurobiol* **9**, 305–313.

Zucker RS & Fogelson AL (1986). Relationship between transmitter release and presynaptic calcium influx when calcium enters through discrete channels. *Proc Natl Acad Sci U S A* **83**, 3032–3036.

Acknowledgements

We would like to express our particular gratitude to John Clements (Canberra, Australia) and Ian Forsythe (Leicester, UK) for critical reading and very helpful comments on an earlier version of the manuscript. The technical assistance of Mrs Przezdziecki is highly appreciated. This study was supported by the DFG (Deutsche Forschungsgemeinschaft, Project Grant SFB515-B2 to RG).